Computational and Structural Biotechnology Journal 19 (2021) 2775–2789

COMPUTATIONAL AND STRUCTURAL BIOTECHNOLOGY JOURNAL

journal homepage: www.elsevier.com/locate/csbj

Employing hypoxia characterization to predict tumour immune microenvironment, treatment sensitivity and prognosis in hepatocellular carcinoma

Fanhong Zeng [a,b], Yue Zhang [a,b], Xu Han [a,b], Min Zeng [a,b], Yi Gao [a,b,1,*], Jun Weng [a,b,1,*]

[a] Department of Hepatobiliary Surgery II, Guangdong Provincial Research Center for Artificial Organ and Tissue Engineering, Guangzhou Clinical Research and Transformation Center for Artificial Liver, Institute of Regenerative Medicine, Zhujiang Hospital, Southern Medical University, Guangzhou, Guangdong Province, China
[b] State Key Laboratory of Organ Failure Research, Southern Medical University, Guangzhou, China

ARTICLE INFO

Article history:
Received 4 February 2021
Received in revised form 24 March 2021
Accepted 25 March 2021
Available online 21 April 2021

Keywords:
Hepatocellular carcinoma
Hypoxia
Gene set enrichment analysis
Tumor immune microenvironment
Risk model
Treatment sensitivity
Prognostic

ABSTRACT

The hypoxic microenvironment was recognized as a major driving force of the malignant phenotype in hepatocellular carcinoma (HCC), which contributes to tumour immune microenvironment (TIM) remodeling and tumor progression. Dysregulated hypoxia-related genes (HRGs) result in treatment resistance and poor prognosis by reshaping tumor cellular activities and metabolism. Approaches to identify the relationship between hypoxia and tumor progression provided new sight for improving tumor treatment and prognosis. But, few practical tools, forecasting relationship between hypoxia, TIM, treatment sensitivity and prognosis in HCC were reported. Here, we pooled mRNA transcriptome and clinical pathology data from the International Cancer Genome Consortium (ICGC) and The Cancer Genome Atlas (TCGA), and later developed a hypoxia risk model including four HRGs (*DCN, DDIT4, PRKCA and NDRG1*). The high-risk group displayed poor clinical characteristics, a malignant phenotype with carcinogenesis/proliferation pathways activation (*MTORC1 and E2F*) and immunosuppressive TIM (decreased immune cell infiltrations and upregulated immunosuppressive cytokines). Meanwhile, activated B cells, effector memory CD8 T cells and *EZH2* deregulation were associated with patient's survival, which might be the core changes of HCC hypoxia. Finally, we validated the ability of the hypoxia risk model to predict treatment sensitivity and found high hypoxia risk patients had poor responses to HCC treatment, including surgical resection, Sorafenib, Transarterial Chemoembolization (TACE) and immunotherapy. In conclusion, based on 4 HRGs, we developed and validated a hypoxia risk model to reflect pathological features, evaluate TIM landscape, predict treatment sensitivity and compounds specific to hypoxia signatures in HCC patients.

1. Introduction

Hepatocellular carcinoma (HCC) is the fifth most common cancer in men and the seventh in women worldwide, which causes more than 700,000 deaths annually [1,2]. In 2021, the predicted mortality rate of HCC ranks sixth among men and seventh among women [2]. As a global high-risk cancer, HCC has a high mortality rate due to a lack of effective treatment [3]. To date, surgery and chemotherapy are still considered the first-line therapies for HCC. Recent studies have shown that immunotherapy had been successful in many advanced cancers, including advanced HCC [4,5]. However, only some patients were sensitive to immunotherapy, which might be assigned to the highly variable immune landscape in HCC patients. Thus, an in-depth understanding of the tumour immune status in HCC is of great importance, to select sensitive treatment and improve prognosis.

Hypoxia is an important factor to promote tumour cell proliferation and tumour progression. Meanwhile, hypoxia is related to maintaining the malignant phenotype of tumour [6]. Recently, the association between hypoxia and tumour microenvironment (TME) has received increasing attention. Insufficient blood supply is an inevitable phenomenon in tumour progression, which results in hypoxia conditions [7,8]. Different from normal cells, tumour

* Corresponding authors at: Department of Hepatobiliary Surgery II, Guangdong Provincial Research Center for Artificial Organ and Tissue Engineering, Guangzhou Clinical Research and Transformation Center for Artificial Liver, Institute of Regenerative Medicine, Zhujiang Hospital, Southern Medical University, Guangzhou, Guangdong Province, China.
E-mail addresses: drgaoy@126.com (Y. Gao), 362593672@qq.com (J. Weng).
[1] These authors are co-responding authors.

https://doi.org/10.1016/j.csbj.2021.03.033
2001-0370/

cells show the characteristics of evolution under a hypoxic environment and develop into a more malignant tendency (i.e, excessive proliferation, invasion and metastasis) [9]. The interaction between hypoxia and TME has been confirmed in various cancers, such as glioma, breast cancer, pancreatic cancer and lung cancer [10–13]. In HCC, hypoxic microenvironment significantly correlates with anti-apoptosis, hyperproliferation, tumour recurrence and metastatic potential, inducing and maintaining malignant phenotype, consequently leading to poor prognosis [14,15]. Previous evidence showed that hypoxia activates the *PI3K/AKT* signalling pathway, which leads to cancer cell proliferation and radiotherapy-resistance [16]. Besides, hypoxia activates the *PLAGL2-EGFR-HIF-1/2α* signalling loop, promoting the progress of HCC and reducing the sensitive response to the *EGFR* drug Erlotinib [17]. Meanwhile, increasing evidence indicated hypoxia reconstructs the tumour immune microenvironment (TIM), such as decreased the proportion of immune cells (i.e, activated CD8 T cells and NK cells) [18] and contributed to the expression of immunosuppressive cytokines (e.g., *EZH2, CCL28, PDL1* and *PD1*) [18]. Although there was a tendency between hypoxia and tumour progression, few studies employed a practical hypoxia model to predict HCC progression, TIM reshaping and therapy sensitivity.

Here, we developed and validated a hypoxia risk model (including four hypoxia-related genes *DCN, DDIT4, PRKCA* and *NDRG1*) to reflect HCC TIM, predict prognosis, evaluate treatment sensitivity and therapeutic compounds which may provide guidance for precise and effective HCC treatment in the future.

2. Materials and methods

2.1. Data acquisition

HCC RNA-seq transcriptome data and clinical information were performed on five separate series. The first series consisted of 231 patients from ICGC (https://icgc.org/) as the training set. The second dataset was obtained from TCGA (https://portal.gdc.cancer.gov/) including 377 patients as a validation set. Ninety-one patients from GSE9843, 268 from GSE25097, and 225 from GSE14520 were downloaded as other validation sets. We used the "SVA" package in R for batch correction before data analysis [20]. GSE6764 (75 patients), GSE109211 (140 patients), and GSE104580 (147 patients) were included in the study to analyze tumour progression, surgical resection, sorafenib and Transarterial Chemoembolization (TACE) sensitivity. Information of patients, including age, gender, and other information were concluded in Tables 2–4.

Survival analysis of sorafenib treatment obtained from Kaplan-Meier Plotter (https://kmplot.com/analysis/index.php?p=service&cancer=liver_rnaseq). TCGA immunohistochemical pictures and single-cell sequencing were obtained from the HPA database (https://www.proteinatlas.org/). ImmuCellAI (http://bioinfo.life.hust.edu.cn/ImmuCellAI#!/) was used to predict the patient's immunotherapy response [21,22]. Besides, the data from TCGA and GEO databases are freely available to the public, and our research also strictly followed access policies and publication guidelines, therefore our study did not require ethical review and approval from an Ethics Committee.

2.2. Hypoxia-risk model constitution

To quantify the effects of hypoxia, 200 hypoxia-related genes were downloaded from Gene Set Enrichment Analysis (hallmark-hypoxia). The differentially expressed hypoxia-related genes ($p < 0.05$, $|\text{Log2-fold change (FC)}| > 1$) were analyzed by univariable and multivariable Cox regression. Where N = 4, the model achieved the coefficients. The differentially expressed genes (DEGs) related to hypoxia between normal and HCC were identified with limma, an R package. The applied formula is as follows:

$$\text{RiskScore} = \sum_{i=1}^{\Pi}(Coefi \times Genei)$$

2.3. Gene set enrichment analyses (GSEA)

The GSEA analysis was performed by GSEA software (version 4.0.3). We utilized it to detect the difference in the set of genes expressed between the high-risk and low-risk group in the enrichment of the MSigDB Collection (h.all.v7.2.symbols.gmt). For each analysis, gene set permutations were performed 1000 times.

2.4. Data analysis

Continuous variables were summarized as the mean ± standard deviation (SD). Chi-square test was used to predict correlation of gene and clinical traits. Differences between groups were compared by the Wilcox test through R software. Different hypoxia subtypes were compared by using the Kruskal–Wallis test. The ConsensusClusterPlus software package in R software was used for consistent clustering to determine the subgroup of HCC samples from GSE14520. The Euclidean squared distance metric and the K-means clustering algorithm were used to divide the sample into k clusters from k = 2 to k = 9. About 80% of the samples were selected at each iteration, and after 100 iterations, the results were obtained [23]. The results were presented in the form of heatmaps of the consistency matrix generated by heatmap R package, and the optimal number of clusters was determined by the consistent cumulative distribution function (CDF) graph.

We utilized Kaplan-Meier analysis to compare the overall survival (OS) between the high and low hypoxia risk groups via survival and survminer packages in R. The significance of survival time differences was calculated using the log-rank test with a threshold of p-value < 0.05. Univariate and multivariate analyses of clinical pathology were performed with Cox regression and then sought an independent risk factor for OS in HCC. To evaluate the accuracy of the model, we utilized the receiver operating characteristic (ROC) curve and calculated the AUC via the survival ROC package in R.A Decision Curve Analysis (DCA) was employed to evaluate the efficacy of using the complex model as a decision-maker tool [24,25]. Also, the calibration curve was used to evaluate the accuracy of the nomogram.

2.5. Estimation of immune cell type

We used the ssGSEA (single-sample gene-set enrichment analysis) algorithm to quantify the relative abundance of immune cell infiltration. The gene set stores a variety of human immune cell subtypes, such as activated CD8 T cells, activated dendritic cells, NK cells, etc [26,27]. The enrichment score calculated by ssGSEA analysis was used to indicate the relative abundance of immune infiltrated cells in each sample.

2.6. Gene–gene interaction network and protein-protein interaction (PPI) network

The gene-gene interaction network was structured by the Gene Multiple Association Network Integration Algorithm (GeneMANIA; https:// www.genemania.org/). STRING database (https://cytoscape.org/) was used to construct a protein–protein interaction network (PPI).

2.7. Identifying the potential inhibitors targeting the hypoxia signatures

The Connectivity Map (CMap) is a database based on gene expression developed by the Broad Institute, which is mainly used to reveal the functional connection between small molecule compounds, genes and disease states [28,29]. Both in ICGC and TCGA database, the top 300 genes included 150 up-regulated genes and 150 down-regulated genes were queried in the CMap tools to investigate therapeutic compounds for HCC. Compounds with an enrichment score of less than −90 or more than 90 were selected as potential inhibitors specific to hypoxia signatures.

2.8. Tissue microarray

We employed HCC tissue microarray (HLivH180Su10) from ShGnghGi Outdo Biotech company, which containing 93 paired HCC and paracancerous tissue to further confirm the relation between genes, prognosis and clinical features (detail were shown in Supplement Table 1). Antibody *DCN* (ab268048, Abcam, 1:200), *NDRG1* (ab124689, Abram, 1:500), *DDIT4* (ab223034 Abcam, 1:100), *PRKCA* (ab32376, Abcam, 1:200) were used for IHC according the instructions.

3. Result

3.1. Hypoxia risk signature to predict HCC prognosis

The whole research design was illustrated in Fig. 1. Total 200 hypoxia-related gene set was downloaded from Gene Set Enrichment Analysis (hallmark-hypoxia). Forty-four differentially expressed hypoxia-related genes (HRGs) ($p < 0.05$ and $|logFc|>1$) were identified between normal and HCC patients in ICGC database (Fig. 2A). Based on 44 differentially expressed HRGs, we performed univariate cox analysis and found that 15 HRGs were significantly associated with HCC patients' overall survival (OS), including *NDRG1, SLC2A1, CA12, DDIT4, ALDOA, PRKCA, ANXA2, RRAGD, ALDOB, PCK1, NEDD4L, FBP1, EFNA3, DCN and MT2A* (Table 5). To better clarify the relationship of these HRGs, we applied the STRING database to perform PPI network analysis. Fourteen HRGs showed close interaction degrees to each other (except *EFNA3*) (Fig. 2B). Later, we performed multivariate Cox analysis, and four candidate genes were chosen to build the model, which were *NDRG1, DDIT4, PRKCA* and *DCN* (Fig. 2C, Table 6). The Risk-score formula was as follows: RiskScore = $(-0.14428 \times DCN) + (0.18771 \times DDIT4) + (0.36480 \times NDRG1) + (0.3727 \times PRKCA)$. We separated patients into low-risk and high-risk groups based on the median RiskScore.

3.2. Prognostic value of the 4 HRGs (NDRG1, DDIT4, PRKCA and DCN)

To explore the biological functions of these 4 candidate genes, we applied the GeneMANIA database. Four candidate genes showed an intimate interaction with each other (Fig. 2D). In protein expression profile (HPA database), *NDRG1, PRKCA* and *DDIT4* were higher in HCC patients than that in normal patients, while *DCN* was lower in HCC patients rather than normal liver tissue (Fig. S1A). To verify the effectiveness of 4 HRGs in predicting prognosis, we performed consistent clustering and identified two new clusters based on *DCN, DDIT4, NDRG1* and *PRKCA* expression (GSE14520). The clustering outcome was stable when k = 2, which appeared to fit with the selection based on clustering stability increasing from k = 2 to 9 (Fig. S1 B-C). Principal component analysis (PCA) analysis showed that cluster analysis could successfully divide HCC patients into two clusters (Fig. S1D). Meanwhile, the heatmap showed that all these 4 HRGs were closely related to tumour progression indexes including tumour size and TMN staging (Fig S1E).

Subsequently, we employed a tissue microarray to evaluate the relationship between protein expression level and OS (Fig. S3). According to our database, we identified these genes that showed different protein-expression in HCC (Fig. 2E). Then we divided patients into a high protein-expression group and a low protein-expression group based on the results of histochemistry. We found that these 4 HRGs were closely related to HCC pathological features (grade and stage). In the high *DDIT4* expression group, patients showed higher tumour stage and grade, which was consistent with *NDRG1* and *PRKCA*. However, the *DCN* low expression group showed a more aggressive phenotype (higher stage and grade) (Fig. 2F-G). Survival analysis showed patients in low *DDIT4* ($p < 0.001$), *NDRG1* ($p < 0.001$) and *PRKCA* ($p < 0.001$) expression had significantly longer OS than those in the high-expression group, while patients in the *DCN* high-expression group ($p < 0.001$) had significantly longer OS than those in low-expression group (Fig. 2H).

Therefore, the above results indicated that these four HRGs (*DCN*, *DDIT4*, *NDRG1* and *PRKCA*) can be used as prognostic indicators.

3.3. Prognostic value and clinic pathological features of the hypoxia risk model in HCC

To further explore the relationship between the hypoxia and clinic pathological features, we examined 4 HRGs (*DCN*, *DDIT4*, *NDRG1* and *PRKCA*) in ICGA and TCGA databases. The boxplot showed the expression of *DDIT4*, *NDRG1* and *PRKCA* increased in the high-risk group in both TCGA and ICGC cohort (Fig. 3A, D), while the expression of *DCN* decreased in the high-risk group. The results indicated that the high-risk group was more prevalent accompanying a higher HRGs expression. Meanwhile, patients with higher RiskScore had more deaths and worse survival in both TCGA and ICGC cohorts (Fig. 3B, C, E, F). To further assess the prognostic value of hypoxia risk model in HCC, we performed a Kaplan-Meier analysis. In ICGC database, the results showed patients in low *NDRG1*, *PRKCA* and hypoxia-risk had significantly longer OS than those in the high expression and hypoxia-risk group ($p < 0.001$, $p = 0.002$, $p < 0.001$). Meanwhile, patients in high *DCN* expression had significantly longer OS than those in the low expression ($p = 0.044$), while there was no difference in the low- and high-expression group of *DDIT4* ($p = 0.192$) (Fig. 3G). In TCGA database, the result showed patients in low *NDRG1* and hypoxia-risk had significantly longer OS than those in the high expression and hypoxia-risk group ($p = 0.011$, $p = 0.033$), while there was no difference in the low and high-expression group of *DCN*, *DDIT4* and *PRKCA* ($p = 0.352$, $p = 0.356$, $p = 0.458$) (Fig. 3H).

Considering the correlation among hypoxia, tumour tumorigenesis and progression, we tried to explore the relationships between hypoxia RiskScore and clinicopathological features. ICGC cohort showed that *NDRG1* expression and hypoxia RiskScore were significantly associated with tumour grade, as the hypoxia RiskScore /gene expression increased with tumour grade. However, *DCN*, *DDIT4* and *PRKCA* expressions showed no significant relationship with tumour grades. Secondly, it showed that *NDRG1* and hypoxia RiskScore were significantly associated with tumour stage/T stage/vascular invasion. As the tumour stage/ T stage/ vascular invasion increased, the *NDRG1* and hypoxia RiskScore / gene expression elevated (Fig. 3I). Analogously, these results were confirmed in TCGA database (Fig. 3J).

Therefore, a hypoxia-risk model closely correlated with prognosis, including survival, tumour progression in HCC.

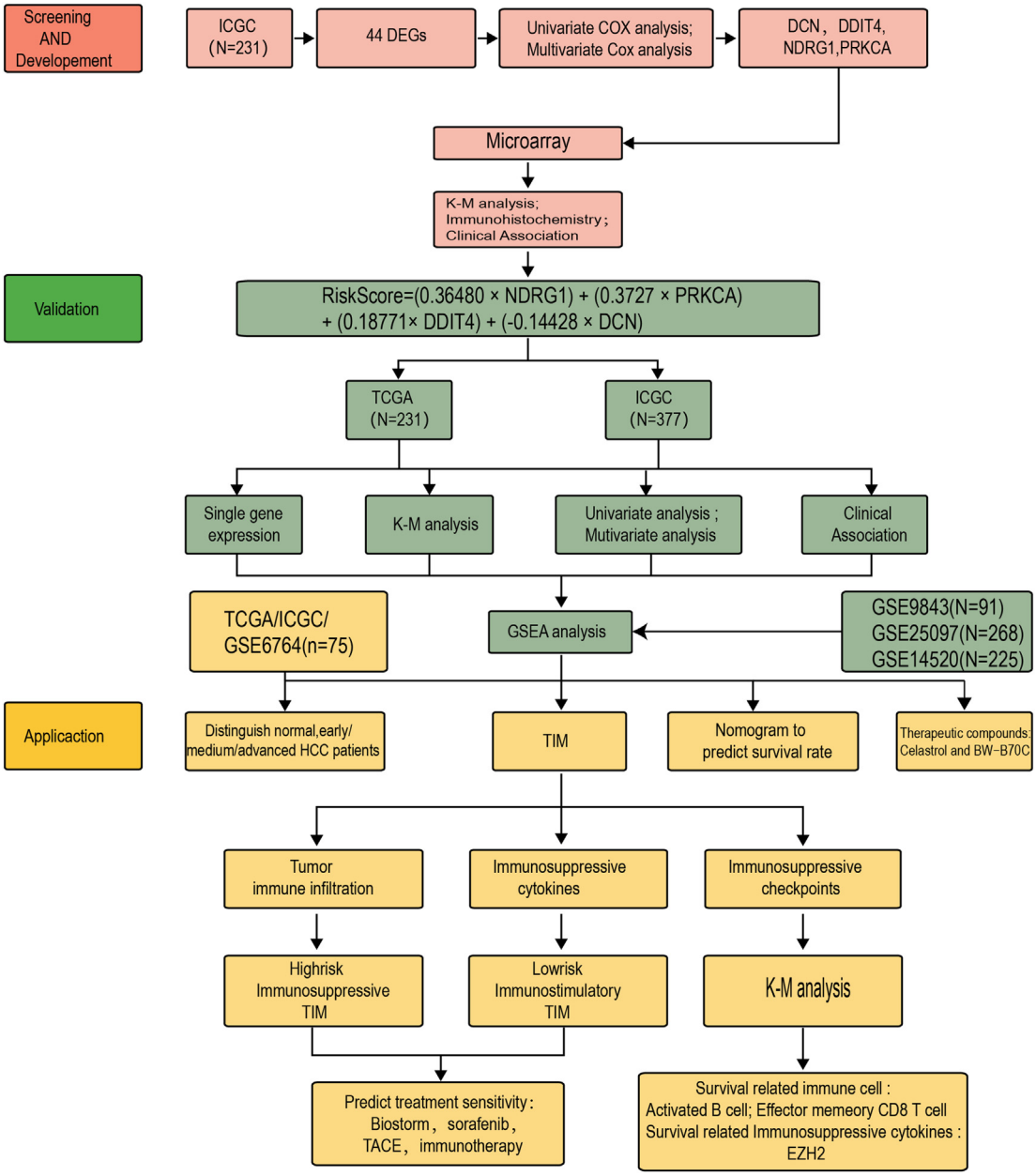

Fig. 1. Establishment, verification, and application of hypoxia risk model.

3.4. Validation of the hypoxia-risk model

To evaluate the predictive accuracy of the hypoxia-risk model in the one-year, two-year, and three-year survival rate, the ROC curve was performed in both ICGC (N = 231) and TCGA (N = 365) database. In ICGC database, the area under the ROC curve (AUC) was 0.809 at one-year, 0.771 at two-year, 0.791 at three-year, which indicated the accuracy and reliability of the model (Fig. 4A). Compared to other factors (*DCN*, *DDIT4*, *PRKCA*, *NDRG1*, age, gender and grade), the hypoxia-risk model had better performance in 1/2/3-year AUC. Besides, risk-model and tumour stage showed similar performance (Fig. 4A-B). In the TCGA database, the AUC of hypoxia-risk model was 0.691 at one-year, 0.628 at two-year, 0.600 at three-year. Consistently, the hypoxia-risk model performed better than other factors (*DCN*, *DDIT4*, *PRKCA*, *NDRG1*, age, gender and grade) in 1/2/3-year AUC. Besides, risk-model and tumour stage showed similar performance (Fig. 4D-E). The above results indicated hypoxia-risk model demonstrated profound accuracy and reliability to predict 1/2/3-year OS.

We further performed univariate and multivariate survival analysis to evaluate the hypoxia-risk model using Cox regression models. In the ICGC dataset, the univariate analysis showed that the hypoxia RiskScore was significantly correlated with OS. Furthermore, multivariate Cox regression analysis indicated that hypoxia RiskScore was also closely related to OS in HCC patients (Fig. 4C). This conclusion was further supported by the TCGA database (Fig. 4F). Therefore, hypoxia-risk model can be identified as an independent prognostic parameter for HCC.

3.5. Hypoxia-risk model to identify HCC tumorigenesis and progression

To identify the efficacy of hypoxia-risk model to distinguish HCC patients from normal patients, we performed a boxplot and identified higher *AFP*/*DDIT4*/*NDRG1*/*PRKCA* expression, hypoxia

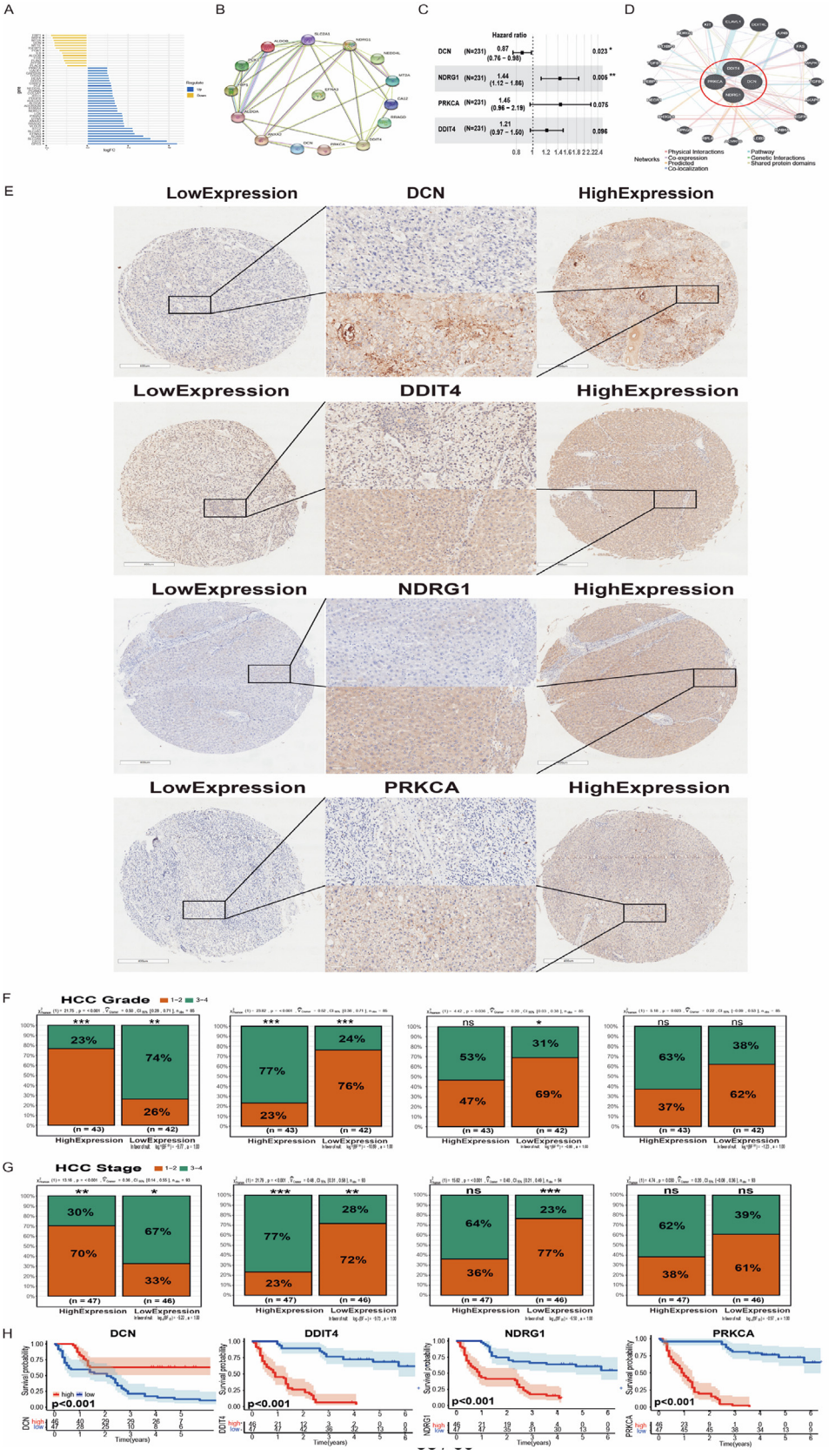

Fig. 2. Characterization of hypoxia to predict prognosis of HCC. (A) Deviation plot of 44 differentially expressed hypoxia-related genes ($p < 0.05$, |logFc|>1); (B) Protein-Protein Interaction interactions among 15 hypoxia-related genes filtered by univariate Cox regression; (C) Construction of a hypoxia-risk model to predict HCC prognosis by multivariate Cox regression; (D) Correlation analysis of four hypoxia genes from GeneMANIA; (E) Immunohistochemistry of *DCN*|*DDIT4*|*NDRG1*|*PRKCA* in tissue microarray (1× and 40×); (F–G) Relationship between *DCN*|*DDIT4*|*NDRG1*|*PRKCA* and clinical characteristics in tissue microarray; (H) Kaplan-Meier analysis of *DCN*|*DDIT4*|*NDRG1*|*PRKCA* in tissue microarray.

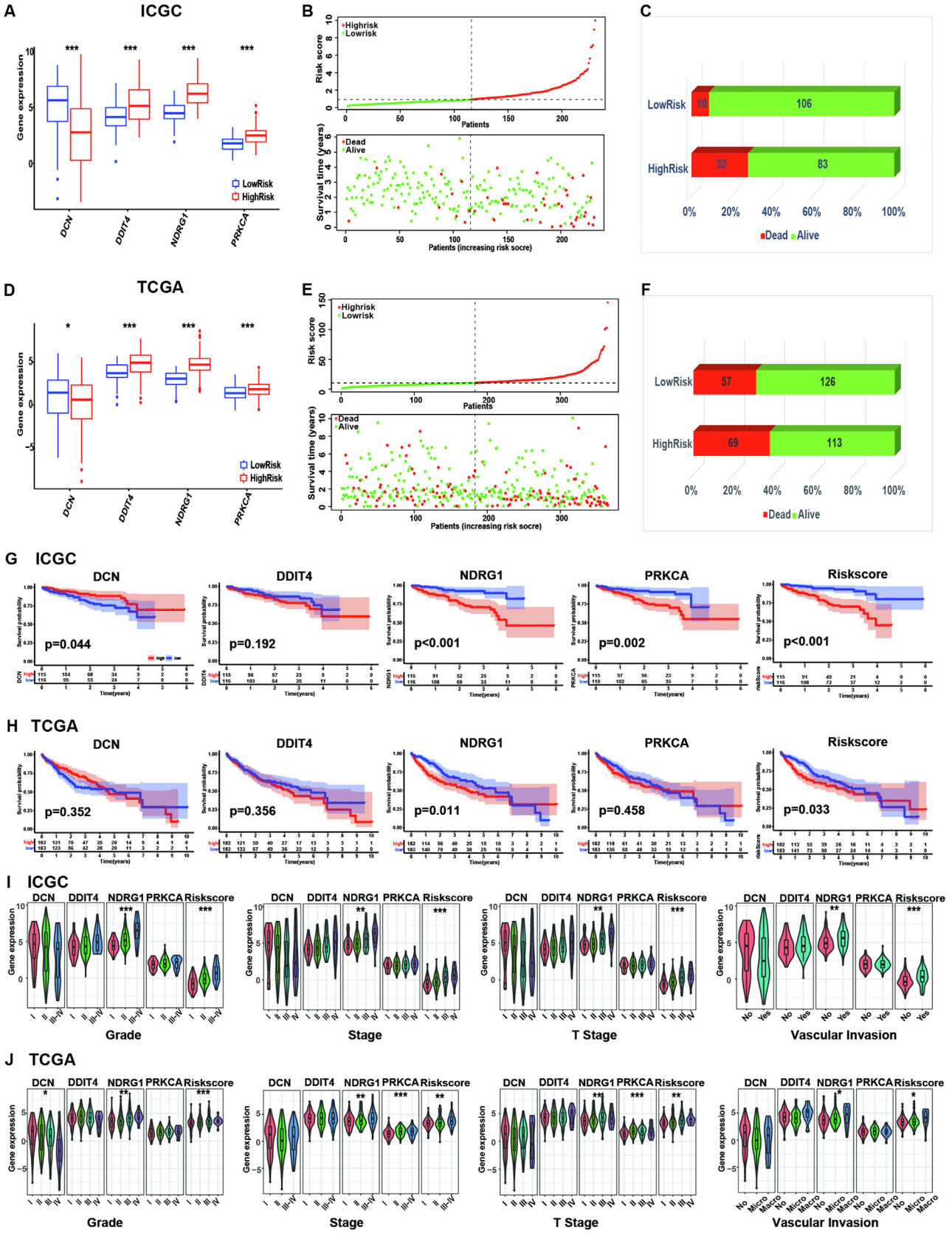

Fig. 3. Prognostic value of the hypoxia risk model in HCC. (A/F) Boxplots showing four hypoxia-related genes expression profiles in high- and low-risk group from ICGC (A) and TCGA (F) database; (B/E) Patient status distribution in the high- and low-risk group from ICGC (B) and TCGA (E) database; (C–F) Mortality rates of the high- and low-risk group in ICGC (C) and TCGA (F) database; The red dot presents death; the green dot presents alive. (G/H) Overall survival curves for patients with high RiskScore and low RiskScore in ICGC (G) and TCGA database (H); (I–J) The expression levels of *DCN*/*DDIT4*/*NDRG1*/*PRKCA*/RiskScore in HCV-HCC with different clinical characteristics in ICGC (I) and TCGA (J) database. (For interpretation of the references to colour in this figure legend, the reader is referred to the web version of this article.)

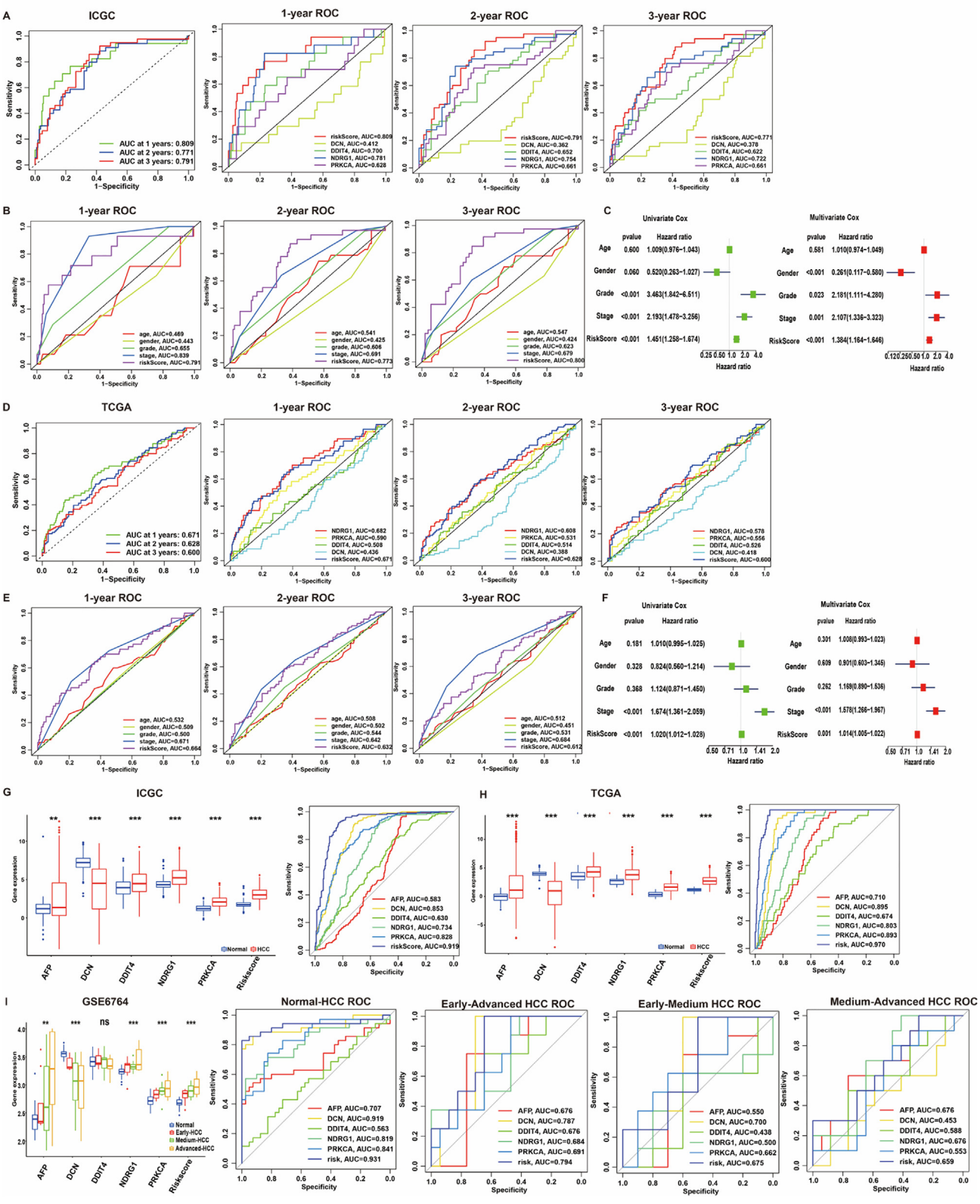

Fig. 4. Validation of hypoxia risk model in HCC. (A-B) ROC curves of ICGC cohort. From left to right: ROC curves showing the predictive accuracy on the one-year, two-year, and three-year survival rate; ROC curves of a single gene on the one-year, two-year, and three-year survival rate; (B) ROC curves of different clinical characteristics on the one-year, two-year, and three-year survival rate; (C) Univariate and Multivariate analyses in ICGC cohort. Left: Univariate analyses evaluating hypoxia signature in terms of OS in HCC patients; Right: Multivariate analyses evaluating the hypoxia signature in terms of OS in HCC patients; (D-E) ROC curves of TCGA cohort. From left to right: ROC curves showing the predictive accuracy on the one-year, two-year, and three-year survival rate; ROC curves of a single gene on the one-year, two-year, and three-year survival rate; (B) ROC curves of different clinical characteristics on the one-year, two-year, and three-year survival rate; (F) Univariate and Multivariate analyses in TCGA cohort. Left: Univariate analyses evaluating hypoxia signature in terms of OS in HCC patients; Right: Multivariate analyses evaluating the hypoxia signature in terms of OS in HCC patients; (G-H) Boxplot and ROC curves (from left to right) of hypoxia-risk model in ICGC (G) and TCGA (H) cohort to distinguish normal and HCC patients; (J) Boxplot and ROC curves (from left to right) of hypoxia-risk model in GEO cohort to distinguish Normal, Early-HCC, Medium HCC and Advanced-HCC patients.

RiskScore and lower *DCN* expression in HCC group of ICGC database. Later, the ROC curve was performed to evaluate the accuracy and reliability of hypoxia-risk model. The results showed hypoxia-risk model (AUC = 0.919) had better performance than regular factor *AFP* (AUC = 0.583) (Fig. 4G). Meanwhile, we repeatedly confirmed these results in TCGA cohort (hypoxia-risk model:0.970; *AFP*:0.710) (Fig. 4H).

To identify whether our model can distinguish HCC progression, we checked *AFP*/*DCN*/*DDIT4*/*NDRG1*/*PRKCA* expressions and hypoxia RiskScore in patients with different HCC statuses including Early/Medium/Advanced HCC (GSE6764). The boxplot showed that hypoxia RiskScore gradually increased in process of Normal-Early HCC-Medium HCC-Advanced HCC. Subsequently, the ROC curve was performed to evaluate the accuracy and reliability of hypoxia-risk model, which had better performance than other indicators (*DCN*, *DDIT4*, *NDRG1*, *PRKCA* and *AFP*) (Fig. 4I). Based on above results, hypoxia-risk model could successfully distinguish different disease states during HCC development.

3.6. GSEA signaling pathways and predicting OS

To find the possible pathway involved in hypoxia, HCC patients were divided into 2 groups to perform GSEA according to hypoxia RiskScore. We took the intersection of the enriched pathways obtained from ICGC, TCGA and GEO databases. Gene sets enriched in the high-risk groups were tumour proliferation in the ICGC database, such as *MTORC1* signalling pathways, *PI3K-AKT-MTOR* signalling, *E2F* targets, and DNA repair signalling pathways (Fig. 5A, Table 7). For instance, activation of both *MTORC1* signalling pathways leads to increased cell proliferation and decreased apoptosis, which finally may contribute to immune cell deficiency because of persistent immune activation [30]. All those activated pathways were proved to be associated with tumour progression and anti-apoptosis. These results were further validated in the TCGA database (Fig. 5B) and the merging GEO database (Fig. 5C).

Based on ICGC database, we built a nomogram combining meaningful clinical characteristics and hypoxia risk model (Fig. 5D). The DCA found that the complex model was more meaningful for predicting clinical survival than the simple model, and our hypoxia model was more effective than other single clinical traits in predicting patients' prognosis (Fig. 5E). And c-index of the complex model was 0.791. The calibration curve confirmed that the nomogram was more reliable for predicting the survival rate of patients at 1, 2, and 3 years (Fig. 5F). All these results indicated a more reliable predictive ability of our hypoxia-related model which can be applied to the clinical area.

3.7. Tumour immune landscape between low and high hypoxia risk HCC patients

To explore the tumour immune landscape among low and high hypoxia-risk groups, we performed ssGSEA. The heatmap of each patient was shown in Fig. S2. Compared to low-risk patients, high-risk patients showed fewer immune cell infiltration in ICGC cohort, such as activated B cells, activated CD8 T cells, effector memory CD8 T cells, NK cells, $CD56^{bright}$ NK cells, $CD56^{dim}$ NK cells, etc. (Fig. 6A, S2A). Analysis of the correlations among the immune cells showed MDSC and regulatory T cells showed the most positive correlation (R = 0.92). Meanwhile, the results showed that there is a close relationship between a variety of immune cells (dendritic cells, B cells, T cells, etc.), such as effector memory CD8 T cells & activated B cells (R = 0.83) (Fig. 6B).

Subsequently, we explored the relationship between our model and immunosuppressive cytokine expression. Based on previous research, we downloaded Cancer-Immunity Cycle associated immunosuppressive cytokines from the Tracking Tumour Immunophenotype website [31]. The boxplot showed that genes involving the negative regulation of the Cancer-Immunity Cycle were mostly upregulated in the high-risk group (Fig. 6C, S2B), indicating that patients had low activities of the Cancer-Immunity Cycle. The correlations among the immunosuppressive cytokines showed *ARG1* and *VEGFA* appeared to have the most negative correlation (R = −0.33), while *CD48* and *BTLA* were the most positive correlation (R = 0.85, Fig. 6D). Besides, ssGSEA also revealed lower ImmuneScore, StromaScore and MicroenvironmentScore, which were closely associated with high hypoxia-risk group (Fig. 6E).

Taken together, the data proved high hypoxia-risk group was closely related to HCC immunosuppressive TIM. The conclusion was also confirmed in TCGA cohort (Fig. 6F-J, S2C, D).

3.8. Hypoxia risk model indicates survival-related immune cells and immunosuppressive cytokines

To further explore the relationship between immune landscape and OS, we performed a Kaplan-Meier analysis. In ICGC cohort, the result showed that patients with decreased activated B cells (p = 0.002) /effector memory CD8 T cells (p = 0.002) were associated with worse OS. Meanwhile, patients with higher expression of *DNMT1* (p = 0.047) /*EZH2* (p < 0.001) were associated with worse OS (Fig. 6K). Analogously, in TCGA cohort the result also showed that patients with less activated B cells (p = 0.016) / effector memory CD8 T cells (p = 0.031) were associated with worse OS. Besides, patients with higher expression of *DNMT1* (p = 0.025) / *EZH2* (p < 0.001) were related to worse OS (Fig. 6L).

Based on HPA database, single-cell sequencing in liver showed *DNMT1* and *EZH2* are enriched in T cells and B cells (Fig. 7A). Therefore, we hypothesized that immune cells and immunosuppressive cytokines work together to influence patient outcomes. To explore the relationship between OS-related factors (activated B cells, effector memory CD8 T cells, *DNMT1* and *EZH2*), we performed the logistic regression analysis. The results showed activated B cell infiltration (ICGC: R = −0.6, p < $2.2e^{-16}$; TCGA: R = −0.21, p = $1.3e^{-05}$), effector memory CD8 T cell infiltration (ICGC: R = −0.61, p < $2.2e^{-16}$; TCGA: R = −0.26, p = $5.5e^{-08}$), *DNMT1* expression (ICGC: R = 0.4, p < $2.2e^{-16}$; TCGA: R = 0.54, p < $2.2e^{-16}$), *EZH2* expression (ICGC: R = 0.69, p < $2.2e^{-16}$; TCGA: R = 0.61, p < $2.2e^{-16}$) were significantly associated with hypoxia RiskScore. As the RiskScore increased, activated B cell infiltration and effector memory CD8 T cell infiltration decreased, *EZH2* expression and *DNMT1* expression elevated (Fig. 7 B-C). Meanwhile, we found *EZH2* expression was significantly associated with activated B cell infiltration (ICGC: R = −0.31, p = $4.6e^{-11}$; TCGA: R = −0.2, p = $5e^{-05}$) and effector memory CD8 T cell infiltration (ICGC: R = −0.33, p = $6.5e^{-13}$; TCGA: R = −0.34, p = $1.3e^{-12}$). However, *DNMT1* expression has no connection with activated B cell infiltration and effector memory CD8 T cell infiltration both in ICGC and TCGA database (Fig. 7 D-E).

Taken together, these results indicated activated B cells, effector memory CD8 T cells and *EZH2* may form a TIM regulating system contributing to HCC TIM remodeling, which might be potential new targets for HCC therapy.

3.9. Model predicts the HCC treatment effectiveness and therapeutic compounds

Surgical resection, Sorafenib and Transarterial chemoembolization (TACE) are traditional proved approaches for HCC treatment, and immunotherapy emerges as a new promising approach for HCC. Therefore, we explored whether hypoxia risk model could predict Sorafenib, Biostorm (Surgical resection plus sorafenib) and TACE treatment sensitivity in HCC. To assess the relationship between progression-free survival (PFS) and RiskScore after sorafe-

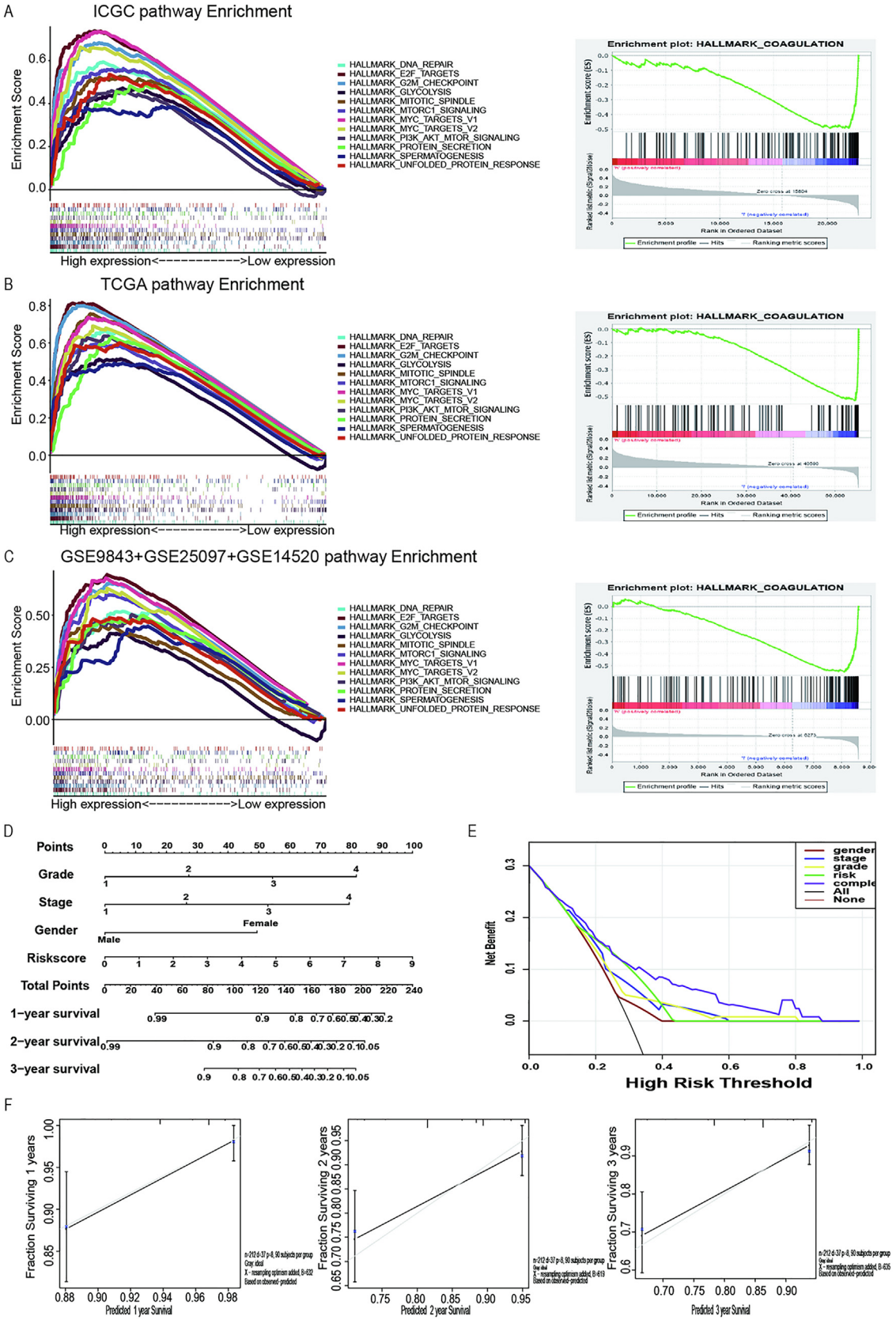

Fig. 5. GSEA enrichment between low- and high-risk groups. (A-C) GSEA showing that enriched hallmarks in ICGC (A), TCGA (B) and GEO (C) cohort. Left: Hallmarks enrich in high-risk group; Right: Hallmark enrich in low-risk group; Normalized enrichment score (NES) > 1 and nominal p-value (NOM p-Val) < 0.05 were considered significant gene sets. (D) Multivariate nomogram predicts survival rate in HCC patients; (E) Decision Curve Analysis (DCA) curves of the nomogram for 1-, 2- and 3-year OS prediction in HCC to evaluate the clinical decision-making benefits of the nomogram; (F) Calibration curve for nomogram.

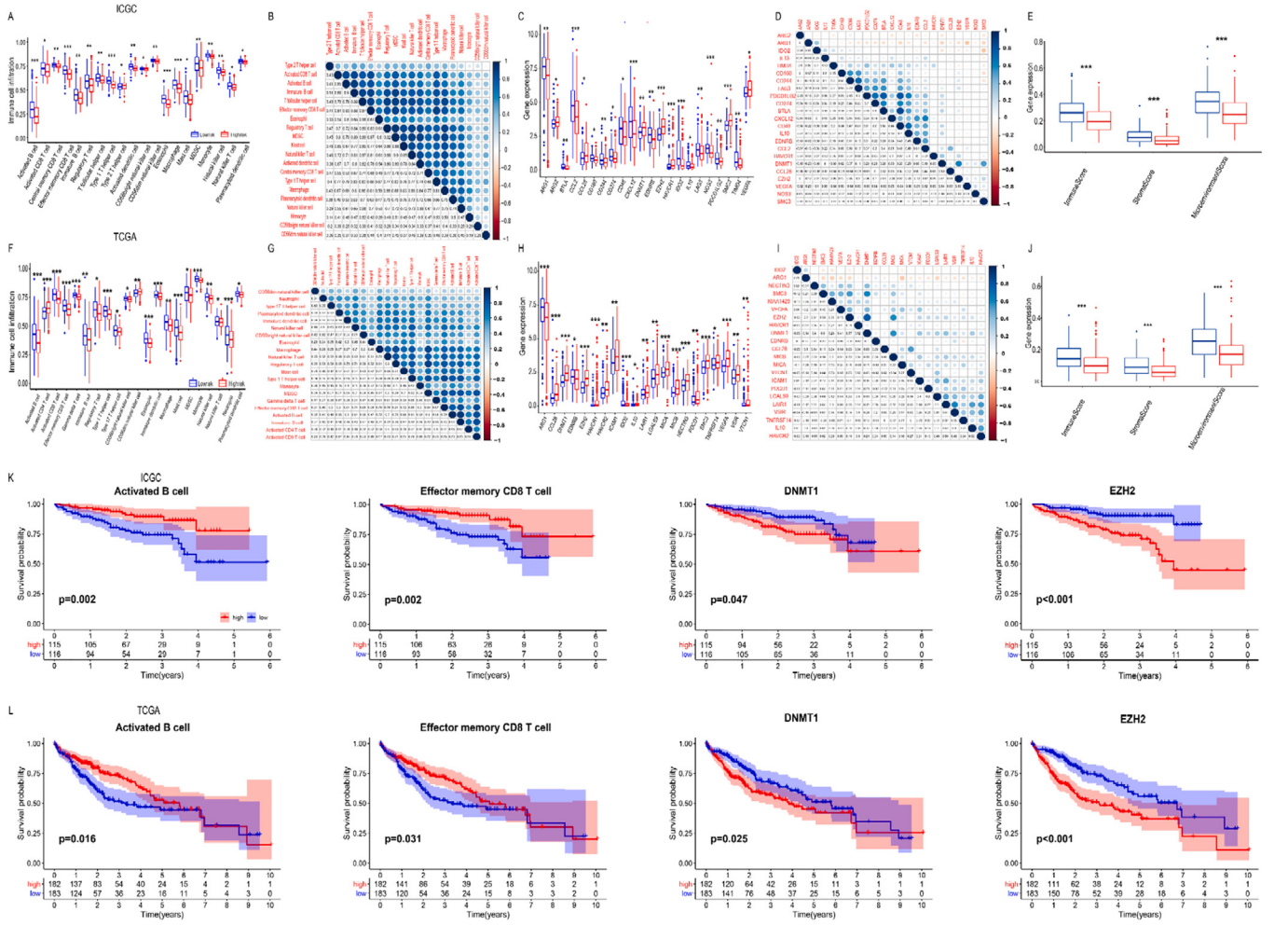

Fig. 6. Immune landscape between low and high hypoxia risk HCC patients. (A/F) Boxplots visualizing the difference of immune cell infiltration between high-risk group and low-risk group in ICGC (A) and TCGA (F) database. * P < 0.05, ** P < 0.01, *** P < 0.001; (B/G) Correlation analysis of immune cells from ICGC (B) and TCGA (G) database; (C/H) Boxplots visualizing the difference of immunosuppressive cytokines between high-risk group and low-risk group in ICGC (C) and TCGA (H) database. * P < 0.05, ** P < 0.01, *** P < 0.001; (D/I) Correlation analysis of immunosuppressive cytokines from ICGC (D) and TCGA (I) database; (E/J) Boxplots showing relationship between RiskScore and immune microenvironment scores in ICGC (E) and TCGA database (J); (K/L) Kaplan–Meier analysis of immune cell infiltration/immunosuppressive cytokines for OS between high-risk group and low-risk group in ICGC (K) and TCGA (L) database.

nib therapy, we performed a Kaplan-Meier analysis and found high-risk group had a shorter recurrence time and poor prognosis compared with low-risk group (Fig. 7F). For Biostorm therapy, the results showed significantly upregulated *DDIT4*, *NDRG1*, and *PRKCA* expression and RiskScore in non-response group, while *DCN* showed no difference between non-response and response group (Fig. 7G). Meanwhile, the result showed TACE non-response group had a higher hypoxia RiskScore than the TACE response group. Besides, significantly upregulated *DDIT4*, *NDRG1*, and *DCN* expressions were also observed in non-response group, while *PRKCA* showed no difference between non-response and response group (Fig. 7H).

Based on above results indicated our model might predict HCC TIM, we further consider whether this model could predict the patient's response to immunotherapy. Previous studies have shown that the ImmunCellAI website could be employed to predict HCC patient's response to immunotherapy [21], we explored whether if our model had consistent ability. The results showed *DCN*, *NDRG1*, *PRKCA*, and RiskScore significantly upregulated in immunotherapy non-response group, while *DDIT4* showed no difference between non-response and response group (Fig. 7I). This phenomenon may be on account that hypoxia can produce immunotherapy resistance by regulating multiple pathways (such as *WNT/NOTCH/EMT* pathway) and stimulating immune cells to secrete multiple cytokines (such as *TGF-β*, *IL4* and *IL6*) [32]. Meanwhile, based on CMap database, the results showed that Celastrol and BW-B70C may serve as therapeutic compounds for HCC (Fig. 7J).

Besides, to explore our model whether be of value for other tumors, we performed a pan-cancer analysis. Compared with HCC, the results showed model-related genes (*DCN, DDIT4, NDRG1* and *PRKCA*) change significantly in cervical squamous cell carcinoma and endocervical adenocarcinoma (CESC), head and neck squamous cell carcinoma (HNSC), lung adenocarcinoma (LUAD) and uveal melanoma (UVM) with similar trends (Fig. S4A). For above cancers, fewer hypoxia models were reported to predict prognosis and treatment approaches. We performed a survival analysis, and results showed our model had a great ability in predicting patients' survival status (Fig. S4B). Therefore, this model could provide effective predictions for CESC, HNSC, LUAD, UVM and HCC diagnosis and treatment.

4. Discussion

Although therapeutic level of HCC has exhibited continuous improvement, HCC keeps high mortality because of scarce specific symptoms for early diagnosis, common therapy resistance and low

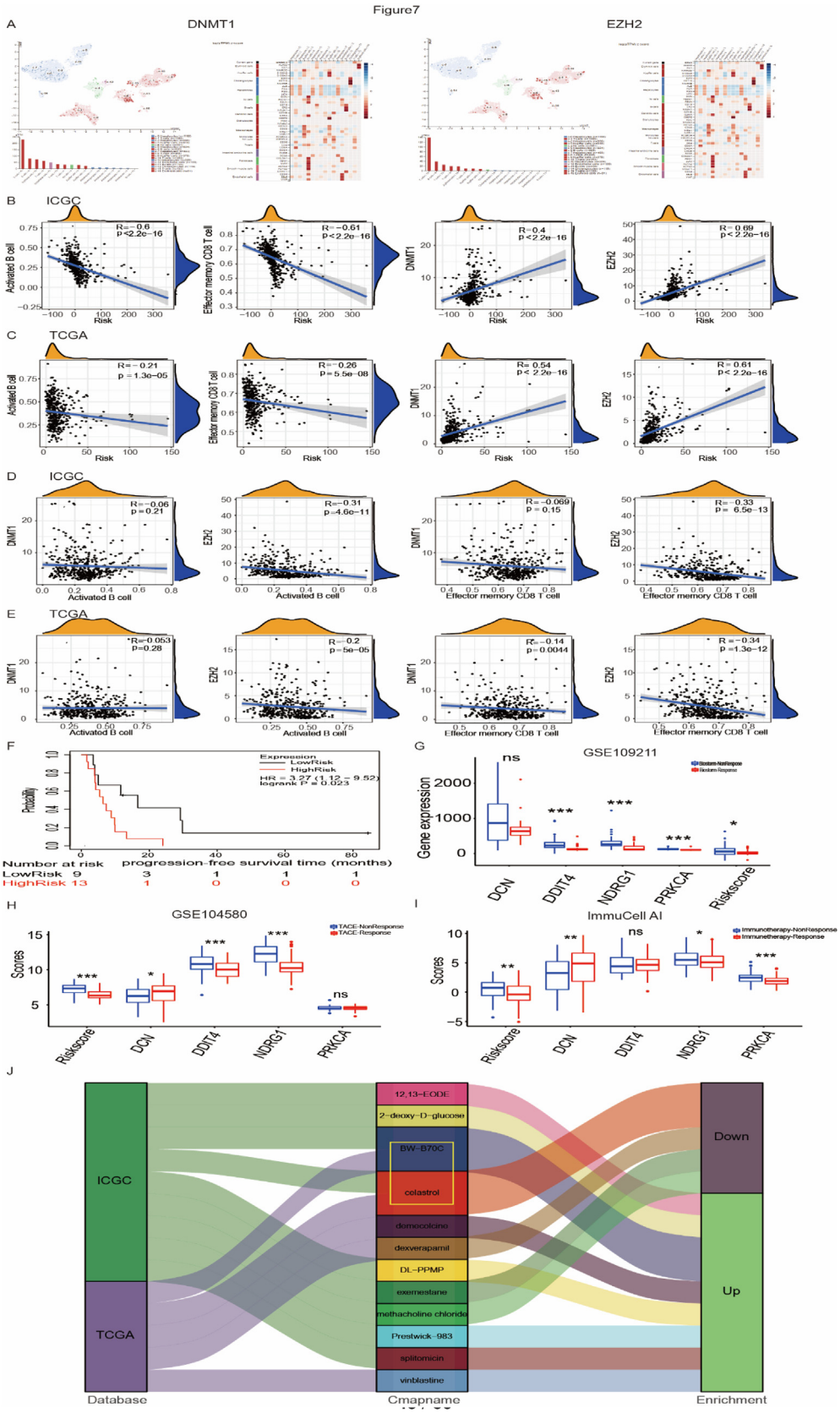

Fig. 7. Immune microenvironment prediction and therapy prediction. (A) Single-cell sequencing showing relationship between *DNMT1*/*EZH2* and immune cells based on HPA database; (B-C) Diagram showing the correlation between RiskScore and activated B cell infiltration/effector memory CD8 T cell infiltration / *DNMT1*/ *EZH2* in ICGC (B) and TCGA (C) database; (D-E) Diagram showing the correlation between activated B cell infiltration/effector memory CD8 T cell infiltration and *DNMT1*/ *EZH2* in ICGC (D) and TCGA (E) database; (F) Recurrence-free survival time after sorafenib treatment between high- and low-risk groups; (G) RiskScore and 4 hypoxia-related genes' expression (*DCN*, *DDIT4*, *NDRG1*, *PRKCA*) between sorafenib non-response group and sorafenib response group; (H) RiskScore and 4 hypoxia-related genes' expression (*DCN*, *DDIT4*, *NDRG1*, *PRKCA*) between TACE non-response group and TACE response group; (I) RiskScore and Four hub genes' expression (*DCN*, *DDIT4*, *NDRG1*, *PRKCA*) between immunotherapy non-response group and immunotherapy response group; (J) Connectivity map analysis (CMap) showing potential inhibitors targeting the HCC hypoxia signatures.

immunotherapy response. Up to now, HCC diagnosis mainly relies on imaging examination and liver biopsy, which lacks ability to precisely assess disease status, evaluate TIM and predict treatment sensitivity. Therefore, a convenient assessment model to evaluate prognosis and treatment sensitivity is urgently needed.

Substantial data suggest that hypoxia is involved in promoting tumorigenesis [33], progression [34], and maintenance of malignant phenotype [35]. For example, the pressure of hypoxia provides an adaptation process of tumour cells reprogramming, contributing to proliferation, migration and invasion [36–38]. Studies also confirmed that hypoxia plays an important role in reprogramming TIM [39–42]. Given the crucial role of hypoxia in tumour progression, a hypoxia-signature model was established that could understand latent molecular mechanisms and improve prognosis in HCC.

Here, we established a hypoxia-risk model based on 4 HRGs (*NDRG1*, *PRKCA*, *DDIT4*, and *DCN*) filtered by ICGC database. In our patient microarray, we found these 4 HRGs closely related to HCC progression and prognosis. Decorin (*DCN*) expressing in fibroblast and myofibroblasts, acts as a soluble pan-receptor tyrosine kinase inhibitor and negatively regulates kinds of growth factor receptors to impede tumorigenesis [43]. DNA damage-inducible transcript 4 (*DDIT4*) is a key mediator of the *MTOR* pathway and promotes tumour growth [44]. N-myc downstream regulated 1(*NDRG1*) engages in a loop between cancer-associated fibroblast and *FOXQ1*/*NDRG1* axis, which contributes to HCC initiation [45]. Moreover, protein kinase C alpha (*PRKCA*) is combined with *DNAJB1*, subsequently increases cAMP-dependent protein kinase (*PKA*) activity, and eventually triggers and potentiates HCC formation [46]. Therefore, we tried to establish hypoxia risk model consisted of these four HRGs (*NDRG1*, *PRKCA*, *DDIT4*, and *DCN*), and tested them in a large-scale patient sequence. Compared with a single gene, our risk model showed profound ability in predicting tumour pathological features (tumour grade, stage, vascular invasion and progressive classification) and patients' prognosis.

Except for driving HCC malignant progression (44), hypoxia protects tumour cells from identification and elimination by the host immune system, ultimately contributing to tumour escape and immune resistance [42]. For example, T cells and NK cells play the most important role in potent antitumour immunity. Hypoxia directly downregulated *PTPROT* expression in HCC-infiltrating T cells, which decreased T effector cell quantity and increased Treg differentiation [47]. Besides, *HIG2* activates the *STAT3* signalling pathway under hypoxia conditions, which promotes *IL-10* release and ultimately inhibits NK cell killing activity [19]. Consistent with previous reports, our hypoxia-risk model can distinct different TIM characterizations. The ssGSEA indicated low-risk group was characterized by the activation of immunity, corresponding to immune-activated phenotype. High-risk group was characterized by the suppression of immunity, corresponding to immune-desert phenotype. We further detected the correlations between different cell types and found MDSC and regulator T cells appeared to have a high positive correlation in ICGC (R = 0.92) and TCGA database (R = 0.89). Meanwhile, the results showed most of the correlation coefficients between various immune cells in the immune system are>0.3, such as effector memory CD8 T cells & activated B cells (R = 0.83).

Meanwhile, NK cells are important immune cells in the body and are the core cells of the natural immune system. They are mainly distributed in the peripheral blood, liver and spleen [48,49]. According to the expression level of CD56, the surface molecule of NK cells, it can be divided into two important functional subtypes: $CD56^{dim}$ NK cells and $CD56^{bright}$ NK cells [50,51]. In terms of function, $CD56^{dim}$ NK cells are mainly cytotoxic and have stronger killing activity. $CD56^{bright}$ NK cells can produce a large number of cytokines, which mainly play a role in immune regulation [52,53]. The liver is an important immune organ of the body, $CD56^{bright}$ NK cells are the dominant NK cell subtype, which mainly secrete IFN, TNF, IL-10, IL-13 and GM-CSF to kill target cells and play a role in immune regulation [54,55]. Previous evidence suggested that the imbalance of NK cells plays an important role in the development and progression of HCC [56–59]. Therefore, we used the hypoxia model to explore changes in NK cell subtypes in the liver. Integrating the results of TCGA and ICGC database, it was found that the total number of NK cells and $CD56^{bright}$ NK cells showed a decreasing trend. Meanwhile, the infiltration of natural killer T cells (NKT cells) also showed a downward trend. At present, tumor immunotherapy mainly focuses on NK cells and T cells to enhance the recognition of tumor surface antigens and prevent tumor immune escape [60,61]. The main reason why the immunotherapy effect of HCC has not reached the ideal effect is the heterogeneity of patients and the immune escape [19,57,62,63]. These results suggest that our model can also be used to distinguish immune cell subtypes and immune microenvironments in different patients, which may facilitate the selection of immunotherapy methods in the future.

Besides, immune cytokines also play an important role in tumour immune microenvironment remodelling [64].In both ICGC and TCGA databases, increased immunosuppressive cytokines (*CCL28, DNMT1, EZH2, SMC3* and *VEGFA*) were identified in high-risk group, which might directly or indirectly regulate immune cells. The above results indicated hypoxia serves as a predominate reshaped TIM as an organism rather than simply changing a single or small portion of immune cells. Meanwhile, different immune cells also interact with each other to determine the overall immune environment via direct contact and cytokines paracrine, which further contributes to suppressive immune status.

Subsequently, survival and correlation analysis indicated activated B cells, effector memory CD8 T cells and *EZH2* might be the core change factors in hypoxia TIM reshaping. Effector memory CD8 T cell is an important subtype of T cell. Previous reports have confirmed that effector memory CD8 T cells can prolong the survival time of patients by secreting *IL-33* [65]. Besides, previous studies showed densities of both T and B cells are associated with HCC patient survival, and interaction between T cells and B cells is critical in the activation of immune response and controlling tumour progression [66–69]. Enhancer of zeste 2 polycomb repressive complex 2 subunit (*EZH2*) could mediate trimethylation on histone 3 lysine 27 (H3K27me3). Abnormal activation of *EZH2* reshaped TIM, influencing tumour cell growth, patients' survival, and tumour metastasis [70–72,75]. Therefore, less activated B cell/effector memory CD8 T cell infiltration and high expression of *EZH2* may be the core factors in creating immunosuppressive tumour microenvironments, which may induce tumour immune escape and immunotherapy resistance.

HCC therapies mainly include chemotherapy, surgery and immunotherapy. Sorafenib, as a first-line drug for HCC, directly target *MAPK/ERK* pathway, *VEGF* receptor tyrosine kinase signalling and other targets, which inhibit tumour growth through antiproliferative and antiangiogenic [73]. In our research, we explored the efficacy of hypoxia risk model in predicting sorafenib sensitivity. The results showed patients with high RiskScore were more frequent in sorafenib resistance. Meanwhile, patients in high-risk group had limited response both in Biostorm (Surgical resection plus sorafenib) and TACE treatment compared with those in low-risk group. Immunotherapy is now recognized as the most promising therapy for cancer. However, the biggest problem is to effectively and precisely distinguish the immunotherapy sensitivity of patients. Since hypoxia model could evaluate TIM and prognosis in HCC, we further explored whether hypoxia-risk model could be employed for evaluating HCC treatment sensitivity. Compared to immunotherapy response patients, results showed immunotherapy

no-response HCC patients had a higher RiskScore. This phenomenon may be on account that most of the immune cells of the high-risk group showed a significant decline, and the prerequisite for immunotherapy is to have a sufficient amount of immune cell infiltration, which may be the main reason why the high-risk group shows low response to immunotherapy. Combining the analysis of immune microenvironment and previous studies, it suggested that this may be due to the decreased infiltration of immune cells, such as activated B cell, effector memory CD8 T cells, activated CD8 T cells and NK cells [74]. Meanwhile, we identified hypoxia signatures and candidate compounds (Celastrol and BW-B70C) targeting HCC from the CMap database. Besides, the pan-cancer analysis indicated that our model can also be used to predict survival for other cancers, such as CESC, HNSC, LUAD and UVM.

In summary, the hypoxia model that we constructed through the ICGC and TCGA databases showed great ability in predicting HCC progress and prognostic. Firstly, the model we constructed can accurately predict pathological features (TMN stage, grade, and vascular invasion), progression (early, medium and advanced stages) and prognostic survival status. Secondly, this hypoxia model could evaluate the tumor immune microenvironment status of HCC patients and find possible targets for the treatment of HCC (activated B cells, effector memory CD8 T cells and EZH2). Thirdly, this model could also be used to evaluate therapy sensitivity of HCC (such as chemotherapy, surgery and immunotherapy). Finally, we screened out two possible drugs (Celastrol and BW-B70C) for the treatment of HCC. Therefore, this hypoxia model could provide powerful insights for future treatment options by evaluating the specific conditions of HCC patients.

At the same time, the hypoxia model also has its limitations. Firstly, the underlying mechanism of the therapeutic targets (activated B cells, effector memory CD8 T cells and EZH2) obtained through model evaluation is not yet clear. Whether there were specific pathways between these targets and the upstream and downstream regulation mechanism still need to further explore. Secondly, the drugs (Celastrol and BW-B70C) we screened out through the model still need to be experimentally explored in the future.

5. Conclusion

In conclusion, we developed and validated a prognostic and treatment sensitivity model based on hypoxia risk in HCC. Firstly, this hypoxia risk model included four hypoxia-associated genes that could serve as an independent prognostic factor for HCC patients. Secondly, this model could reflect the tumour immune landscape within the cancerous tissue. The research also indicated activated B cells, effector memory CD8 T cells and *EZH2* might be the core change factors in hypoxia TIM remodeling, which provided a possible treatment target for HCC patients with high hypoxia risk. Besides, our model also predicted therapy sensitivity (such as chemotherapy, surgery and immunotherapy) and therapeutic compounds (Celastrol and BW-B70C), which may guide hypoxia-targeted therapies for HCC patients in the future.

CRediT authorship contribution statement

Fanhong Zeng: Supervision. **Yue Zhang:** . **Xu Han:** . **Min Zeng:** . **Yi Gao:** . **Jun Weng:** .

Declaration of Competing Interest

The authors declare that they have no known competing financial interests or personal relationships that could have appeared to influence the work reported in this paper.

Acknowledgements

We thank Dr. Xiaoping Xu and Yuan Chen for their help in the discussion on the field of hypoxia and immunotherapy of HCC.

Funding

This work was supported by the National Key R&D Program of China (2018YFC1106400; 2018YFA0108200); Science and Technology Planning Project of Guangdong Province (2015B020229002), the National Natural Science Foundation of China (31972926); The Natural Science Foundation of Guangdong Province (2014A030312013, 2018A030313128); Guangdong key research and development plan (2019B020234003); Science and Technology Program of Guangzhou (201803010086); Guangdong Basic and Applied Basic Research Foundation (2021A1515011040).

Availability of data and materials

Not applicable.

Ethics approval and consent to participate

Not applicable.

Consent for publication

Not applicable.

Appendix A. Supplementary data

Supplementary data to this article can be found online at https://doi.org/10.1016/j.csbj.2021.03.033.

References

[1] Sharma SA, Kowgier M, Hansen BE, Brouwer WP, Maan R, Wong D, et al. Toronto HCC risk index: a validated scoring system to predict 10-year risk of HCC in patients with cirrhosis. J Hepatol 2018;68(1):92–9.
[2] Torre LA, Bray F, Siegel RL, Ferlay J, Lortet-Tieulent J, Jemal A. Global cancer statistics, 2012. CA: A Cancer J Clin 2015;65:87–108.
[3] Siegel RL, Miller KD, Jemal A. Cancer statistics, 2020. CA: A Cancer J Clin 2020;70:7–30.
[4] El-Khoueiry AB, Sangro B, Yau T, Crocenzi TS, Kudo M, Hsu C, et al. Nivolumab in patients with advanced hepatocellular carcinoma (CheckMate 040): an open-label, non-comparative, phase 1/2 dose escalation and expansion trial. Lancet 2017;389(10088):2492–502.
[5] Zhu AX, Finn RS, Edeline J, Cattan S, Ogasawara S, Palmer D, et al. Pembrolizumab in patients with advanced hepatocellular carcinoma previously treated with sorafenib (KEYNOTE-224): a non-randomised, open-label phase 2 trial. Lancet Oncol 2018;19(7):940–52.
[6] Chen G, Gu H, Fang T, Zhou K, Xu J, Yin X. Hypoxia-induced let-7f-5p/TARBP2 feedback loop regulates osteosarcoma cell proliferation and invasion by inhibiting the Wnt signaling pathway. Aging. 2020;12(8):6891–903.
[7] Cao Q, Zhou D-J, Pan Z-Y, Yang G-G, Zhang H, Ji L-N, et al. CAIXplatins: highly potent platinum(IV) prodrugs selective against carbonic anhydrase IX for the treatment of hypoxic tumors. Angew Chem Int Ed 2020;59(42):18556–62.
[8] Han Z, Wang Y, Chen Y, Fang H, Yuan H, Shi X, et al. A novel luminescent Ir(iii) complex for dual mode imaging: synergistic response to hypoxia and acidity of the tumor microenvironment. Chem Commun (Camb) 2020;56:8055–8.
[9] Farina AR, Cappabianca L, Sebastiano M, Zelli V, Guadagni S, Mackay AR. Hypoxia-induced alternative splicing: the 11th Hallmark of Cancer. J Exp Clin Cancer Res 2020;39:110.
[10] Lin W, Wu S, Chen X, Ye Y, Weng Y, Pan Y, et al. Characterization of hypoxia signature to evaluate the tumor immune microenvironment and predict prognosis in glioma groups. Front Oncol 2020;10. https://doi.org/10.3389/fonc.2020.00796.
[11] Gibadulinova A, Bullova P, Strnad H, Pohlodek K, Jurkovicova D, Takacova M, et al. CAIX-mediated control of LIN28/let-7 axis contributes to metabolic adaptation of breast cancer cells to hypoxia. Int J Mol Sci 2020;21(12):4299. https://doi.org/10.3390/ijms21124299.
[12] Fuentes NR, Phan J, Huang Y, Lin D, Taniguchi CM. Resolving the HIF paradox in pancreatic cancer. Cancer Lett 2020;489:50–5.

[13] Catarata MJ, Ribeiro R, Oliveira MJ, Robalo Cordeiro C, Medeiros R. Renin-angiotensin system in lung tumor and microenvironment interactions. Cancers (Basel) 2020;12(6):1457. https://doi.org/10.3390/cancers12061457.
[14] Zhang J, Zhang Qi, Lou Yu, Fu Q, Chen Qi, Wei T, et al. Hypoxia-inducible factor-1α/interleukin-1β signaling enhances hepatoma epithelial-mesenchymal transition through macrophages in a hypoxic-inflammatory microenvironment. Hepatology 2018;67(5):1872–89.
[15] Liu Z, Wang Y, Dou C, Xu M, Sun L, Wang L, et al. Hypoxia-induced up-regulation of VASP promotes invasiveness and metastasis of hepatocellular carcinoma. Theranostics 2018;8(17):4649–63.
[16] Bamodu OA, Chang H-L, Ong J-R, Lee W-H, Yeh C-T, Tsai J-T. Elevated PDK1 expression drives PI3K/AKT/MTOR signaling promotes radiation-resistant and dedifferentiated phenotype of hepatocellular carcinoma. Cells 2020;9(3):746. https://doi.org/10.3390/cells9030746.
[17] Hu W, Zheng S, Guo H, Dai B, Ni J, Shi Y, et al. PLAGL2-EGFR-HIF-1/2α signaling loop promotes HCC progression and erlotinib insensitivity. Hepatology 2021;73:674–91.
[18] Terry S, Buart S, Chouaib S. Hypoxic stress-induced tumor and immune plasticity, suppression, and impact on tumor heterogeneity. Front Immunol 2017;8:1625.
[19] Cui C, Fu K, Yang Lu, Wu S, Cen Z, Meng X, et al. Hypoxia-inducible gene 2 promotes the immune escape of hepatocellular carcinoma from nature killer cells through the interleukin-10-STAT3 signaling pathway. J Exp Clin Cancer Res 2019;38(1). https://doi.org/10.1186/s13046-019-1233-9.
[20] Schobert IT, Savic LJ, Chapiro J, Bousabarah K, Chen E, Laage-Gaupp F, et al. Neutrophil-to-lymphocyte and platelet-to-lymphocyte ratios as predictors of tumor response in hepatocellular carcinoma after DEB-TACE. Eur Radiol 2020;30(10):5663–73.
[21] Miao Y-R, Zhang Q, Lei Q, Luo M, Xie G-Y, Wang H, et al. ImmuCellAI: a unique method for comprehensive T-cell subsets abundance prediction and its application in cancer immunotherapy. Adv Sci 2020;7(7):1902880. https://doi.org/10.1002/advs.v7.710.1002/advs.201902880.
[22] Liu C, Hu F, Xia M, Han L, Zhang Q, Guo A. GSCALite: a web server for gene set cancer analysis. Bioinformatics 2018;34:3771-2.
[23] Wilkerson MD, Hayes DN. ConsensusClusterPlus: a class discovery tool with confidence assessments and item tracking. Bioinformatics 2010;26:1572-3.
[24] Vickers AJ, Elkin EB. Decision curve analysis: a novel method for evaluating prediction models. Med Decis Making 2006;26(6):565–74.
[25] Kerr KF, Brown MD, Zhu K, Janes H. Assessing the clinical impact of risk prediction models with decision curves: guidance for correct interpretation and appropriate use. J Clin Oncol 2016;34(21):2534–40.
[26] Charoentong P, Finotello F, Angelova M, Mayer C, Efremova M, Rieder D, et al. Pan-cancer immunogenomic analyses reveal genotype-immunophenotype relationships and predictors of response to checkpoint blockade. Cell Rep 2017;18(1):248–62.
[27] Barbie DA, Tamayo P, Boehm JS, Kim SY, Moody SE, Dunn IF, et al. Systematic RNA interference reveals that oncogenic KRAS-driven cancers require TBK1. Nature 2009;462(7269):108–12.
[28] Lamb J. The Connectivity Map: a new tool for biomedical research. Nat Rev Cancer 2007;7(1):54–60.
[29] Lamb J. The connectivity map: using gene-expression signatures to connect small molecules, genes, and disease. Science 2006;313(5795):1929–35.
[30] Nguyen HD, Chatterjee S, Haarberg KMK, Wu Y, Bastian D, Heinrichs J, et al. Metabolic reprogramming of alloantigen-activated T cells after hematopoietic cell transplantation. J Clin Invest 2016;126:1337-52.
[31] Chen D, Mellman I. Oncology meets immunology: the cancer-immunity cycle. Immunity 2013;39(1):1–10.
[32] Plaks V, Kong N, Werb Z. The cancer stem cell niche: how essential is the niche in regulating stemness of tumor cells?. Cell Stem Cell 2015;16(3):225–38.
[33] Panou V, Røe OD. Inherited genetic mutations and polymorphisms in malignant mesothelioma: a comprehensive review. Int J Mol Sci 2020;21 (12):4327. https://doi.org/10.3390/ijms21124327.
[34] Aggarwal V, Miranda O, Johnston PA, Sant S. Three dimensional engineered models to study hypoxia biology in breast cancer. Cancer Lett 2020;490:124–42.
[35] Yamasaki A, Yanai K, Onishi H. Hypoxia and pancreatic ductal adenocarcinoma. Cancer Lett 2020;484:9–15.
[36] Fernández-Cruz A, Ortega L, García G, Gallego I, Álvarez-Uría A, Chamorro-de-Vega E, et al. Etiology and prognosis of pneumonia in patients with solid tumors: a prospective cohort of hospitalized cases. Oncologist 2020;25(5). https://doi.org/10.1634/theoncologist.2019-0031.
[37] Liu Y, Wu J, Huang W, Weng S, Wang B, Chen Y, et al. Development and validation of a hypoxia-immune-based microenvironment gene signature for risk stratification in gastric cancer. J Transl Med 2020;18(1). https://doi.org/10.1186/s12967-020-02366-0.
[38] Saito Y, Takasawa A, Takasawa K, Aoyama T, Akimoto T, Ota M, et al. Aldolase A promotes epithelial-mesenchymal transition to increase malignant potentials of cervical adenocarcinoma. Cancer Sci 2020;111(8):3071–81.
[39] Wiedenmann N, Grosu A-L, Büchert M, Rischke HC, Ruf J, Bielak L, et al. The utility of multiparametric MRI to characterize hypoxic tumor subvolumes in comparison to FMISO PET/CT. Consequences for diagnosis and chemoradiation treatment planning in head and neck cancer. Radiother Oncol 2020;150:128–35.
[40] Cui G, He P, Yu L, Wen C, Xie X, Yao G. Oxygen self-enriched nanoplatform combined with US imaging and chemo/photothermal therapy for breast cancer. Nanomed Nanotechnol Biol Med 2020;29:102238. https://doi.org/10.1016/j.nano.2020.102238.
[41] Nollet EA, Cardo-Vila M, Ganguly SS, Tran JD, Schulz VV, Cress A, et al. Androgen receptor-induced integrin α6β1 and Bnip3 promote survival and resistance to PI3K inhibitors in castration-resistant prostate cancer. Oncogene 2020;39(31):5390–404.
[42] Maggs L, Ferrone S. Improving the clinical significance of preclinical immunotherapy studies through incorporating tumor microenvironment–like conditions. Clin Cancer Res 2020;26(17):4448–53.
[43] Sainio AO, Järveläinen HT. Decorin-mediated oncosuppression - a potential future adjuvant therapy for human epithelial cancers. Br J Pharmacol 2019;176(1):5–15.
[44] Cheng Z, Dai Y, Pang Y, Jiao Y, Liu Y, Cui L, et al. Up-regulation ofDDIT4 predicts poor prognosis in acute myeloid leukaemia. J Cell Mol Med 2020;24 (1):1067–75.
[45] Luo Q, Wang C-Q, Yang L-Y, Gao X-M, Sun H-T, Zhang Yu, et al. FOXQ1/NDRG1 axis exacerbates hepatocellular carcinoma initiation via enhancing crosstalk between fibroblasts and tumor cells. Cancer Lett 2018;417:21–34.
[46] Xu L, Hazard FK, Zmoos A, Jahchan N, Chaib H, Garfin PM, et al. Genomic analysis of fibrolamellar hepatocellular carcinoma. Human Mol Genet 2015;24:50-63.
[47] Hou J, Deng L, Zhuo H, Lin Z, Chen Y, Jiang R, et al. PTPROt maintains T cell immunity in the microenvironment of hepatocellular carcinoma. J Mol Cell Biol 2015;7(4):338–50.
[48] Kwong Y, Chan TSY, Tan D, Kim SJ, Poon L, Mow B, et al. PD1 blockade with pembrolizumab is highly effective in relapsed or refractory NK/T-cell lymphoma failing l-asparaginase. Blood 2017;129:2437-42.
[49] Gornalusse GG, Hirata RK, Funk SE, Riolobos L, Lopes VS, Manske G, et al. HLA-E-expressing pluripotent stem cells escape allogeneic responses and lysis by NK cells. Nat Biotechnol 2017;35(8):765–72.
[50] Cooper MA, Fehniger TA, Turner SC, Chen KS, Ghaheri BA, Ghayur T, et al. Human natural killer cells: a unique innate immunoregulatory role for the CD56(bright) subset. Blood 2001;97:3146-51.
[51] Jacobs R, Hintzen G, Kemper A, Beul K, Kempf S, Behrens G, et al. CD56bright cells differ in their KIR repertoire and cytotoxic features from CD56dim NK cells. Eur J Immunol 2001;31(10):3121–6.
[52] Ram DR, Manickam C, Lucar O, Shah SV, Reeves RK. Adaptive NK cell responses in HIV/SIV infections: a roadmap to cell-based therapeutics?. J Leukoc Biol 2019;105(6):1253–9.
[53] Zhu H, Blum RH, Bjordahl R, Gaidarova S, Rogers P, Lee TT, et al. Pluripotent stem cell–derived NK cells with high-affinity noncleavable CD16a mediate improved antitumor activity. Blood 2020;135:399-410.
[54] Fang F, Xiao W, Tian Z. Challenges of NK cell-based immunotherapy in the new era. Front Med 2018;12(4):440–50.
[55] Jeong SH, Song H-N, Park JS, Yang D-H, Koh Y, Yoon S-S, et al. Allogeneic stem cell transplantation for patients with natural killer/T cell lymphoid malignancy: a multicenter analysis comparing upfront and salvage transplantation. Biol Blood Marrow Transpl 2018;24(12):2471–8.
[56] Chen Y, Tian Z. HBV-induced immune imbalance in the development of HCC. Front Immunol 2019;10:2048.
[57] Han Q, Zhao H, Jiang Yu, Yin C, Zhang J. HCC-derived exosomes: critical player and target for cancer immune escape. Cells 2019;8(6):558. https://doi.org/10.3390/cells8060558.
[58] Sun C, Sun H-y, Xiao W-H, Zhang C, Tian Z-G. Natural killer cell dysfunction in hepatocellular carcinoma and NK cell-based immunotherapy. Acta Pharmacol Sin 2015;36(10):1191–9.
[59] Liu P, Chen L, Zhang H. Natural killer cells in liver disease and hepatocellular carcinoma and the NK cell-based immunotherapy. J Immunol Res 2018;2018:1–8.
[60] André P, Denis C, Soulas C, Bourbon-Caillet C, Lopez J, Arnoux T, et al. Anti-NKG2A mAb is a checkpoint inhibitor that promotes anti-tumor immunity by unleashing both T and NK cells. Cell 2018;175(7):1731–1743.e13.
[61] Morandi F, Yazdanifar M, Cocco C, Bertaina A, Airoldi I. Engineering the bridge between innate and adaptive immunity for cancer immunotherapy: focus on γδ T and NK cells. Cells 2020;9(8):1757. https://doi.org/10.3390/cells9081757.
[62] Han C, Jiang Y, Wang Z, Wang H. Natural killer cells involved in tumour immune escape of hepatocellular carcinomar. Int Immunopharmacol 2019;73:10–6.
[63] Shin S, Kim M, Lee SJ, Park KS, Lee CH. Trichostatin A sensitizes hepatocellular carcinoma cells to enhanced NK cell-mediated killing by regulating immune-related genes. Cancer Genomics Proteomics 2017;14:349–62.
[64] Tian Y, Li Y, Shao Y, Zhang Y. Gene modification strategies for next-generation CAR T cells against solid cancers. J Hematol Oncol 2020;13:54.
[65] Brunner SM, Rubner C, Kesselring R, Martin M, Griesshammer E, Ruemmele P, et al. Tumor-infiltrating, interleukin-33-producing effector-memory CD8+ T cells in resected hepatocellular carcinoma prolong patient survival. Hepatology 2015;61(6):1957–67.
[66] Garnelo M, Tan A, Her Z, Yeong J, Lim CJ, Chen J, et al. Interaction between tumour-infiltrating B cells and T cells controls the progression of hepatocellular carcinoma. Gut 2017;66(2):342–51.
[67] Driessens G, Kline J, Gajewski TF. Costimulatory and coinhibitory receptors in anti-tumor immunity. Immunol Rev 2009;229:126-44.
[68] Pagès F, Galon J, Dieu-Nosjean M-C, Tartour E, Sautès-Fridman C, Fridman W-H. Immune infiltration in human tumors: a prognostic factor that should not be ignored. Oncogene 2010;29(8):1093–102.

[69] Schneider C, Teufel A, Yevsa T, Staib F, Hohmeyer A, Walenda G, et al. Adaptive immunity suppresses formation and progression of diethylnitrosamine-induced liver cancer. Gut 2012;61(12):1733–43.
[70] Mohammad F, Weissmann S, Leblanc B, Pandey DP, Højfeldt JW, Comet I, et al. EZH2 is a potential therapeutic target for H3K27M-mutant pediatric gliomas. Nat Med 2017;23(4):483–92.
[71] Jin X, Kim LJY, Wu Q, Wallace LC, Prager BC, Sanvoranart T, et al. Targeting glioma stem cells through combined BMI1 and EZH2 inhibition. Nat Med 2017;23(11):1352–61.
[72] Tiwari N, Tiwari V, Waldmeier L, Balwierz P, Arnold P, Pachkov M, et al. Sox4 is a master regulator of epithelial-mesenchymal transition by controlling Ezh2 expression and epigenetic reprogramming. Cancer Cell 2013;23(6):768–83.
[73] Wilhelm SM, Adnane L, Newell P, Villanueva A, Llovet JM, Lynch M. Preclinical overview of sorafenib, a multikinase inhibitor that targets both Raf and VEGF and PDGF receptor tyrosine kinase signaling. Mol Cancer Ther 2008;7(10):3129–40.
[74] Havel JJ, Chowell D, Chan TA. The evolving landscape of biomarkers for checkpoint inhibitor immunotherapy. Nat Rev Cancer 2019;19(3):133–50.
[75] Song Hang et al. Long noncoding RNA CASC11 promotes hepatocarcinogenesis and HCC progression through EIF4A3-mediated E2F1 activation. Clin Transl Med 2020;10(7):e220. https://doi.org/10.1002/ctm2.220.